Electronic Supplementary Information

Thermally Induced Dehydration Reactions of Monosodium L-Glutamate Monohydrate: Dehydration of Solids Accompanied by Liquefaction

Takahiro Okazaki,[1] Masami Hara,[1] Nikita V. Muravyev,[2] and Nobuyoshi Koga[1,*]
[1]Department of Science Education, Division of Educational Sciences, Graduate School of Education, Hiroshima University, 1-1-1 Kagamiyama, Higashi-Hiroshima 739-8524, Japan
[2]Semenov Institute of Chemical Physics, Russian Academy of Sciences, 4 Kosygin Str., 119991, Moscow, Russia.

Contents

* Corresponding author. e-mail: nkoga@hiroshima-u.ac.jp

S1. Sample characterization

Figure S1 shows the textures of the MSG-MH particles with 300–500 μm sieve fractions observed using a stereomicroscope (SZX7, Olympus). The particles exhibited a columnar shape with a long axis (length: 0.5–1.5 mm). The powder XRD pattern of the MSG-MH sample was measured using a RINT-2200V instrument (Rigaku) with monochrome Cu-K_α (40 kV, 20 mA) radiation, scanning 2θ values of 5°–60°, and a step of 0.02°, at a scan speed of 4° min^{-1} (Figure S2). The XRD pattern was consistent with the reference pattern of MSG-MH (orthorhombic, S.G.: $P2_12_12_1(19)$, $a = 17.9560$, $b = 15.2460$, $c = 5.5682$, $\alpha = \beta = \gamma = 90.000$, ICDD PDF 00-029-1787).[S1] The MSG-MH sample was diluted with KBr, and the FT-IR spectrum was recorded using a FT-IR8400S instrument (Shimadzu) in the wavenumber range of 4600–400 cm^{-1} by diffuse reflectance method (Figure S3). The FT-IR spectrum was coincident with that of a database (NIST Chemistry WebBook, SRD 69; https://webbook.nist.gov/cgi/inchi?ID=B6004640&Mask=80#Refs), in which the O–H and N–H stretching bands appeared in the wavenumber region of 3700–2500 cm^{-1}. C–H stretching bands also appeared in the 3300–2800 cm^{-1} region. Absorption bands attributed to various double-bonded chemical groups appeared in the region of 1950–1450 cm^{-1}.

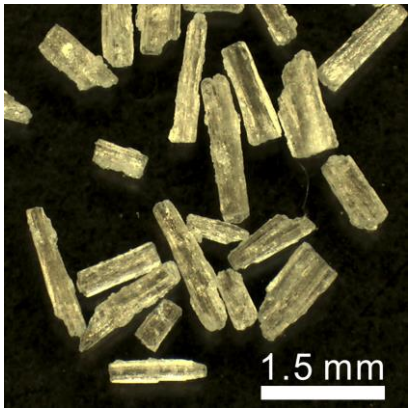

Figure S1. Texture of the MSG-MH particles (300–500 μm sieve fraction).

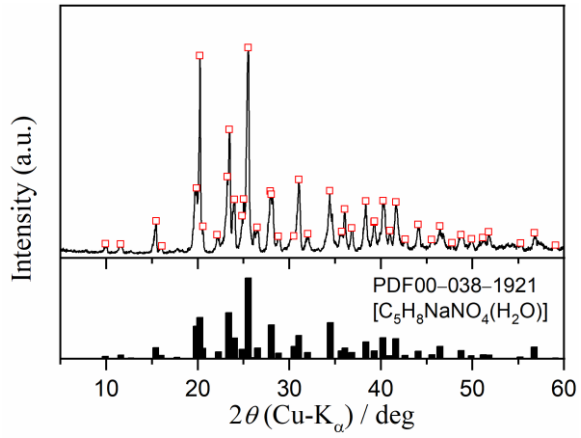

Figure S2. XRD pattern of the MSG-MH sample.

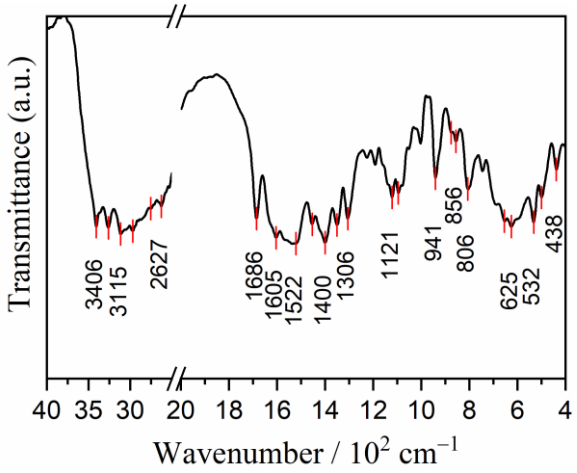

Figure S3. FT-IR spectrum of the MSG-MH sample.

S2. Thermal behavior

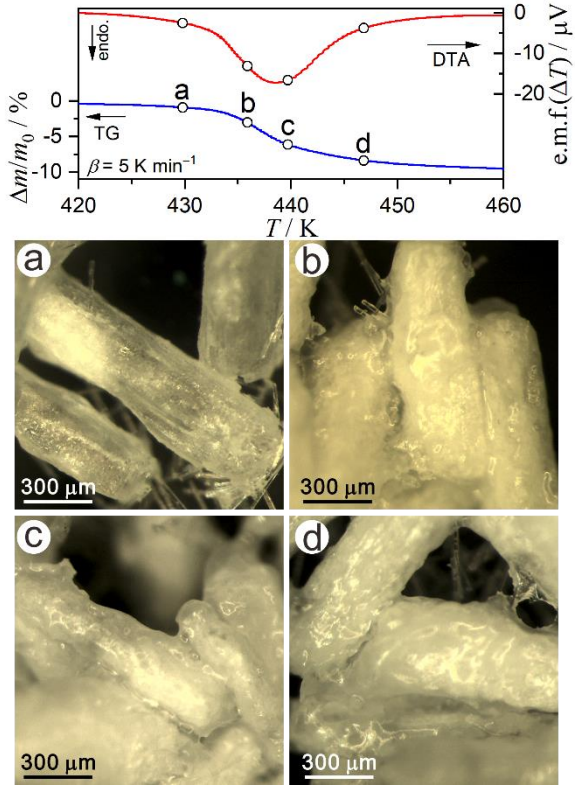

Figure S4. Appearances of the sample particles, once heated to different temperatures at β = 5 K min^{-1} and recovered after cooling to room temperature: (a) T = 430 K (α = 0.05), (b) T = 436 K (α = 0.32), (c) T = 440 K (α = 0.61), and (d) T = 447 K (α = 0.86).

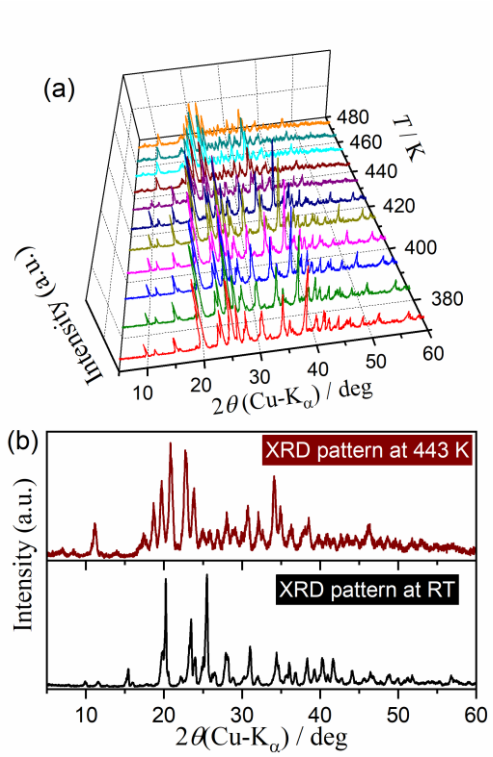

Figure S5. Changes in the XRD patterns during the heating of MSG-MH according to the stepwise isothermal program in a flow of dry N_2 gas (q_v = 100 cm^3 min^{-1}): (a) XRD patterns at different temperatures and (b) comparison of the XRD patterns of the MSG-MH and the product of the first thermal dehydration process.

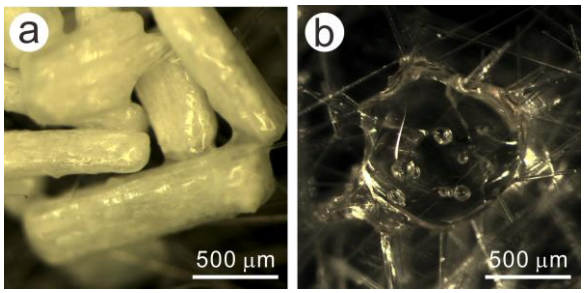

Figure S6. Appearances of the products of the first and second thermal dehydration processes obtained by isothermal heating in a dry N_2 gas flow: (a) product of the first thermal dehydration process obtained at 422 K and (b) product of the second thermal dehydration process obtained at 461 K.

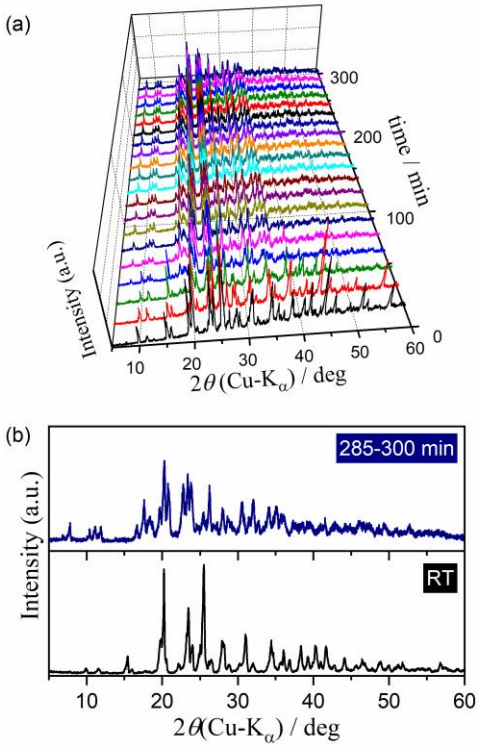

Figure S7. Changes in the XRD patterns during the heating of MSG-MH at 428 K in a flow of dry N_2 gas (q_v = 100 cm^3 min^{-1}): (a) XRD patterns at different heating times and (b) comparison of the XRD patterns of the MSG-MH and the product of the first thermal dehydration process.

S3. Kinetics of the thermal dehydration of crystalline water

S3.1. Kinetic curves

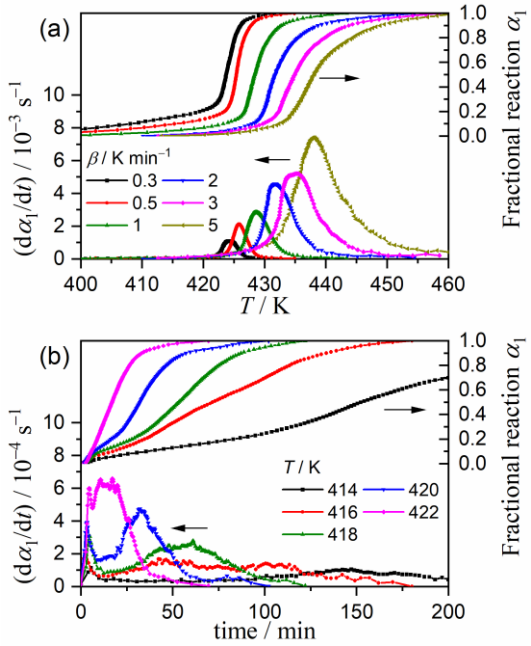

Figure S8. Kinetic curves for the thermal dehydration of crystalline water: (a) linear nonisothermal conditions and (b) isothermal conditions.

S3.2 Mathematical deconvolution analysis

For MDA of the DTG peak for the thermal dehydration of crystalline water (the first mass-loss process), the logistic power peak (LPP) function was used to fit each component DTG peak of the reactions in the low-temperature region, whereas the Weibull function was applied to each component peaks of the reactions in the high-temperature region.

■ LPP function:

$$F(t) = \frac{a_0}{a_3}\left[1+\exp\left(\frac{t+a_2\ln a_3 - a_1}{a_2}\right)\right]^{\frac{-a_3-1}{a_3}} \exp\left(\frac{t+a_2\ln a_3 - a_1}{a_2}\right)(a_3+1)^{\frac{a_3+1}{a_3}}, \quad \text{(S1)}$$

where a_0, a_1, a_2, and a_3 are the amplitude, center, width ($\neq 0$), and shape (≥ 1), respectively.

■ Weibull function:

$$F(t) = a_0\left(\frac{a_3-1}{a_3}\right)^{\frac{1-a_3}{a_3}}\left\{\frac{t-a_1}{a_2}+\left(\frac{a_3-1}{a_3}\right)^{\frac{1}{a_3}}\right\}^{a_3-1} \exp\left[-\left\{\frac{t-a_1}{a_2}+\left(\frac{a_3-1}{a_3}\right)^{\frac{1}{a_3}}\right\}^{a_3}+\frac{a_3-1}{a_3}\right], \quad \text{(S2)}$$

where a_0, a_1, a_2, and a_3 are the amplitude, center, width (>0), and shape (>1.01), respectively.

The typical MDA results for the DTG peaks of the thermal dehydration of the crystalline water in the low- and high-temperature regions are shown in Figure S9. All the DTG curves were fitted satisfactorily by the LPP and Weibull functions for the partially overlapping two and three-step processes in the low- and high-temperature regions, respectively. From the MDA results, the contributions of each component peak to the overall DTG peak were calculated (Table S1). In addition, a series of kinetic curves for each reaction step was generated from the mathematically separated DTG peaks, as shown in Figures S10 and S11, for the reactions in the low- and high-temperature regions, respectively.

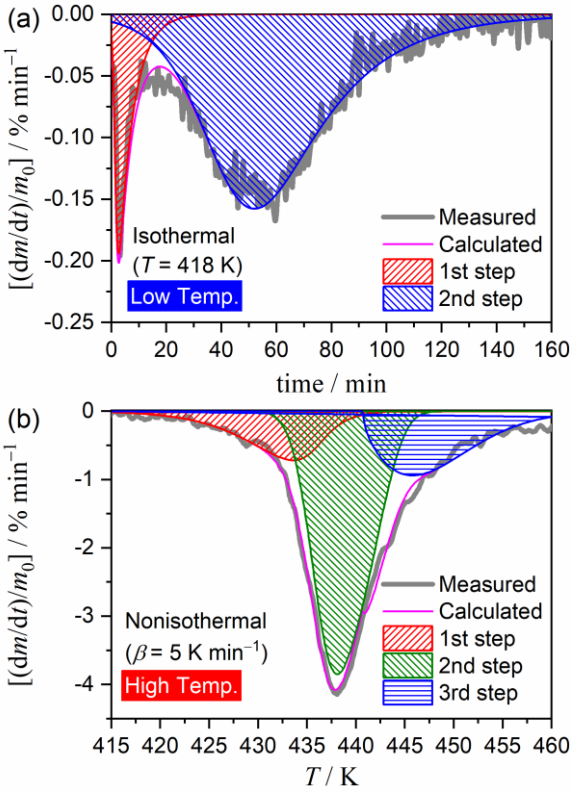

Figure S9. Typical MDA results for the thermal dehydration of crystalline water under (a) isothermal conditions at 418 K and (b) linear nonisothermal conditions at a β of 5 K min^{-1}.

Table S1. Results of the MDA and subsequent formal kinetic analysis of the thermal dehydration of crystalline water

Temp. region	i	$c_{1(i)}$	$E_{a,1(i)}$ / kJ mol^{-1}, [a]	$\frac{d\alpha_{1(i)}}{d\theta_{1(i)}} = A_{1(i)}f(\alpha_{1(i)})$ with $f(\alpha_{1(i)}) = \alpha_{1(i)}^{m_{1(i)}}(1-\alpha_{1(i)})^{n_{1(i)}}[-\ln(1-\alpha_{1(i)})]^{p_{1(i)}}$				
				$A_{1(i)}$ / s^{-1}	$m_{1(i)}$	$n_{1(i)}$	$p_{1(i)}$	R^{2}, [b]
Low	1	0.14 ± 0.87	235.1 ± 19.8	(3.70 ± 0.07) × 10^{26}	−3.18 ± 0.24	2.16 ± 0.09	3.42 ± 0.23	0.9993
	2	0.86 ± 0.01	384.3 ± 9.1	(1.41 ± 0.03) × 10^{45}	5.17 ± 0.17	−0.40 ± 0.06	−4.31 ± 0.16	0.9993
High	1	0.21 ± 0.02	316.0 ± 7.0	(1.46 ± 0.04) × 10^{36}	−0.65 ± 0.31	1.09 ± 0.12	0.64 ± 0.30	0.9992
	2	0.58 ± 0.04	182.5 ± 23.8	(2.26 ± 0.01) × 10^{20}	0.40 ± 0.05	1.00 ± 0.02	0.33 ± 0.05	0.9999
	3	0.20 ± 0.04	103.1 ± 16.3	(2.05 ± 0.01) × 10^{10}	1.17 ± 0.05	0.68 ± 0.02	−0.84 ± 0.04	0.9999

[a]Average value over $0.1 \leq \alpha \leq 0.9$.
[b]Determination coefficient of the nonlinear least-squares analysis for fitting the experimental master plot.

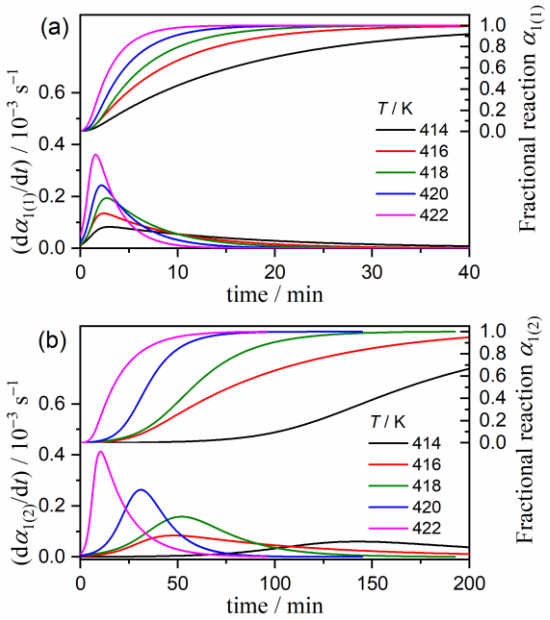

Figure S10. Kinetic curves for the first and second reaction steps of the thermal dehydration of crystalline water under isothermal conditions (low-temperature region): (a) the first and (b) second reaction steps.

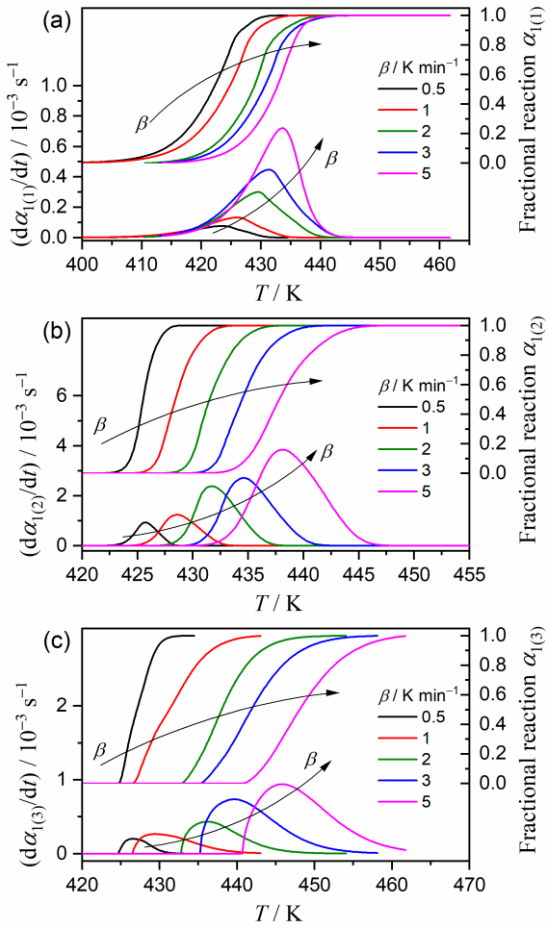

Figure S11. Kinetic curves for the first, second, and third reaction steps of the thermal dehydration of crystalline water under linear nonisothermal conditions (high-temperature region): (a) the first, (b) second, and (c) third reaction steps.

The kinetic curves in Figures S10 and S11 were analyzed using the isoconversional method (eq. (4)). The $E_{a,1(i)}$ values of the reaction step (i) at various $\alpha_{1(i)}$ values, determined from the Friedman plots, are shown in Figure S12. Except for the initial part of the first reaction step in the low-temperature region, the $E_{a,1(i)}$ values changed gradually as the reaction proceeded. The average $E_{a,1(i)}$ values ($0.1 \le \alpha_{1(i)} \le 0.9$) are listed in Table S1. The experimental master plots of $d\alpha_{1(i)}/d\theta_{1(i)}$ versus $\alpha_{1(i)}$ for each reaction step were drawn by calculating according to eq. (9), as shown in Figures S13 and S14 for the reactions in the low and high temperature regions, respectively. The experimental master plots were fitted using SB(n, m, p) (eq. (6)) by optimizing the kinetic exponents and the $A_{1(i)}$ values through nonlinear least-squares analysis. The optimized kinetic exponents and $A_{1(i)}$ are listed in Table S1.

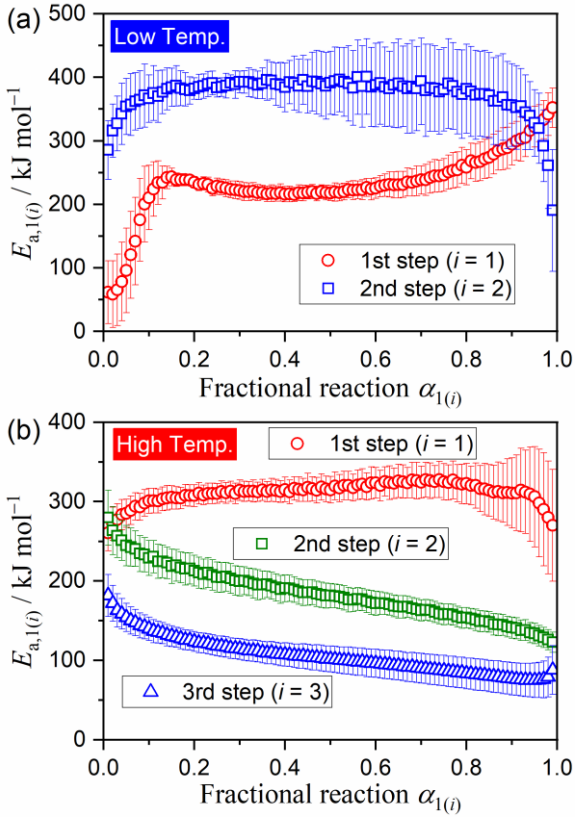

Figure S12. $E_{a,1(i)}$ values at various $\alpha_{1(i)}$ values determined by the Friedman plots applied to the mathematically separated kinetic curves in the (a) low- and (b) high-temperature regions.

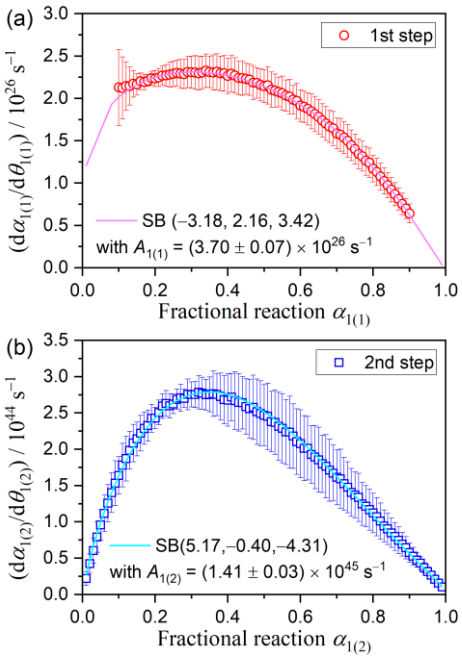

Figure S13. Experimental master plots for each step of the reaction in the low-temperature region: (a) first and (b) second reaction steps.

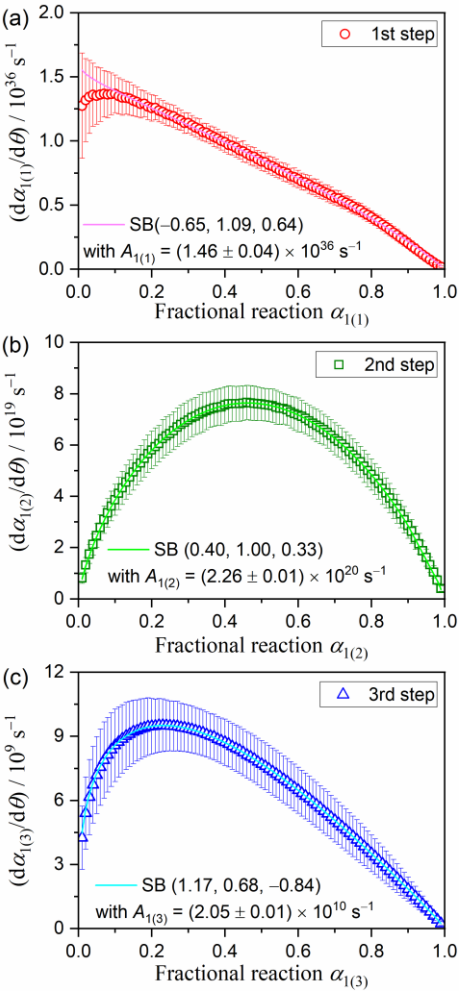

Figure S14. Experimental master plots for each step of the reaction in the high-temperature region: (a) first, (b) second, and (c) third reaction steps.

S4. Kinetics of the thermally induced intramolecular dehydration

S4.1. Kinetic curves

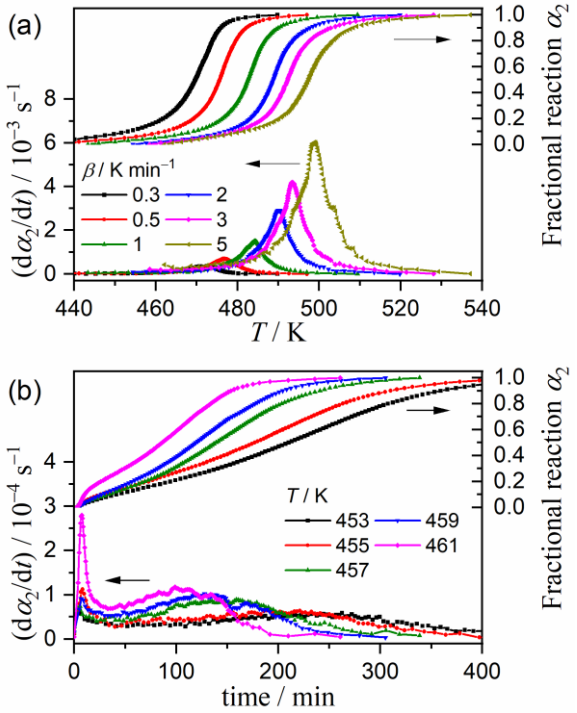

Figure S15. Kinetic curves for the intramolecular dehydration of MSG-AH to form SPyrG: (a) linear nonisothermal conditions and (b) isothermal conditions. The initial rapid mass-loss under isothermal conditions was observed during the temperature rising period to reach the programmed constant temperature.

S4.2. Mathematical deconvolution analysis

The Weuibll function (eq. (S2)) was employed to deconvolute the thermally induced intramolecular dehydration of MSG-AH into two reaction steps (Figure S16). However, the acceleration part of the DTG curve could not be satisfactorily fitted by the Weibull function. Therefore, the acceleration part was fitted as two peaks by the Weibull functions (Figure S16(a)). Thereafter, the first and second peaks, resulting from the three-peak deconvolution, were calculated to simulate the first reaction step (Figure S16(b)), achieving the MDA of the two-step process. The contributions of each reaction step are listed in Table S2. The kinetic curves at different β values, obtained for each reaction step by MDA, are shown in Figure S17. The average $E_{a,2(i)}$ values in the $\alpha_{2(i)}$ range of 0.1–0.9 are listed in Table S2. The experimental master plots for each reaction step drawn using the average values are shown in Figure S19 and the results of fitting using SB(m, n, p) are listed in Table S2.

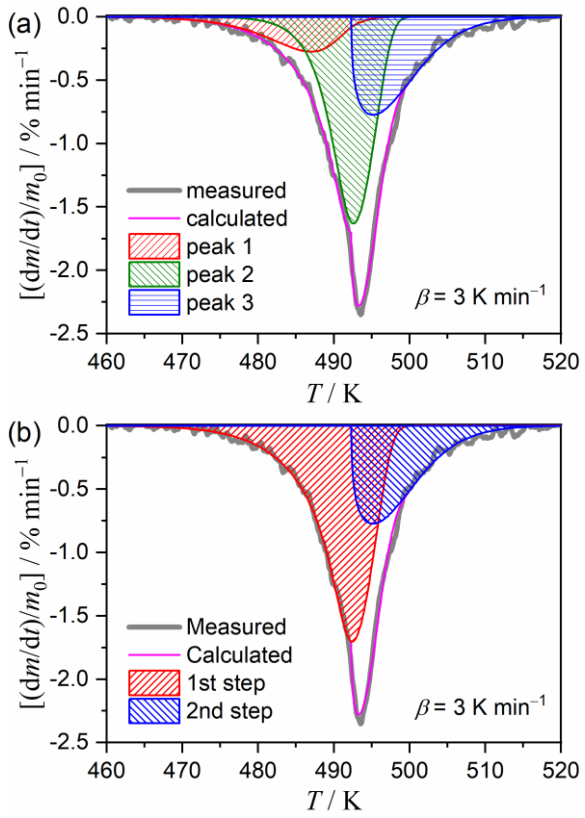

Figure S16. Typical MDA results for the thermally induced intramolecular dehydration of MSG-AH to form SPyrG: (a) deconvolution into three peaks and (b) the expected two-step process simulated by cumulating peaks 1 and 2 in (a) for the first reaction step.

Table S2. Results of the MDA and the subsequent formal kinetic analysis for the thermally induced intramolecular dehydration of MSG-AH under linear nonisothermal conditions

i	$c_{1(i)}$	$E_{a,2(i)}$ / kJ mol^{-1}, [a]	$\frac{d\alpha_{2(i)}}{d\theta_{2(i)}} = A_{2(i)} f(\alpha_{2(i)})$ with $f(\alpha_{2(i)}) = \alpha_{2(i)}^{m_{2(i)}}(1-\alpha_{2(i)})^{n_{2(i)}}[-\ln(1-\alpha_{2(i)})]^{p_{2(i)}}$				
			$A_{2(i)}$ / s^{-1}	$m_{2(i)}$	$n_{2(i)}$	$p_{2(i)}$	R^{2}, [b]
1	0.73 ± 0.04	202.7 ± 2.3	(2.39 ± 0.07) × 10^{19}	−5.18 ± 0.33	2.74 ± 0.13	5.68 ± 0.32	0.9946
2	0.27 ± 0.04	159.6 ± 14.1	(7.73 ± 0.03) × 10^{14}	0.80 ± 0.05	0.87 ± 0.02	–0.50 ± 0.05	0.9999

[a] Average value over $0.1 \le \alpha \le 0.9$.
[b] Determination coefficient of the nonlinear least-squares analysis for fitting the experimental master plot.

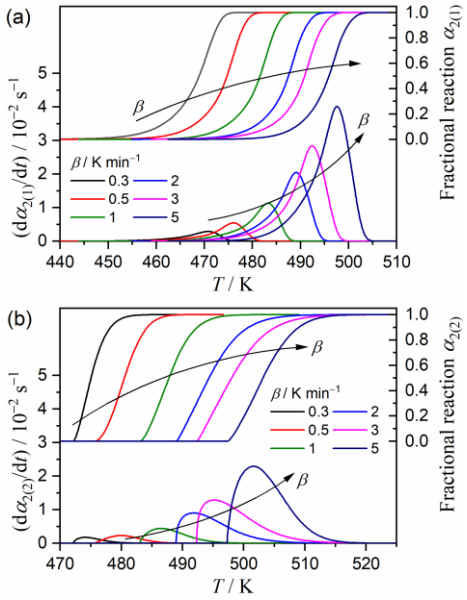

Figure S17. Kinetic curves at different β values for each reaction step of the thermally induced intramolecular dehydration of MSG-AH: (a) first and (b) second reaction steps.

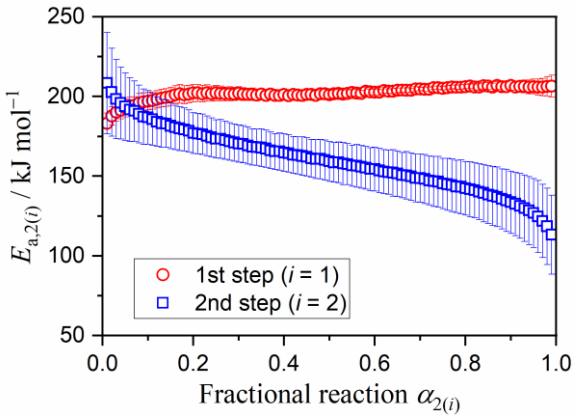

Figure S18. $E_{a,2(i)}$ values at various $\alpha_{2(i)}$ values determined by the Friedman plots applied to the mathematically separated kinetic curves.

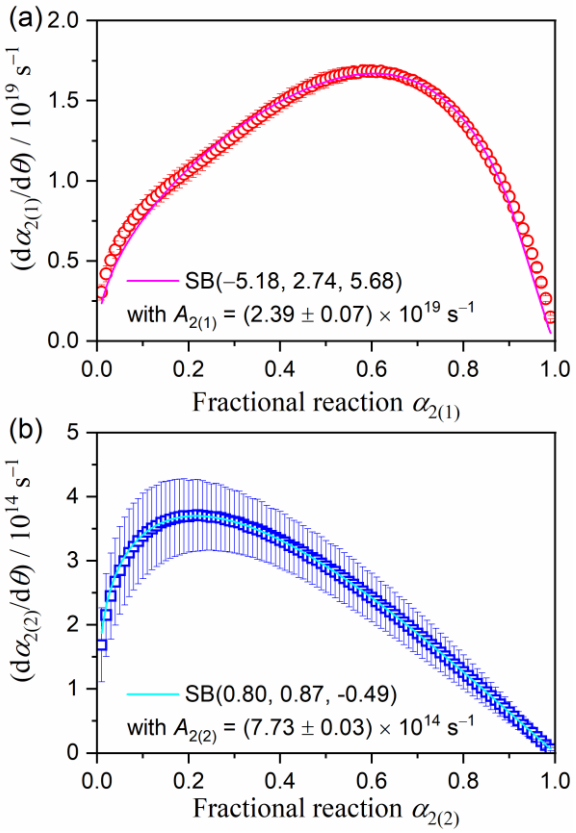

Figure S19. Experimental master plots for each reaction step: (a) the first and (b) second reaction steps.

S4.3. Glass transition of SPyrG glass

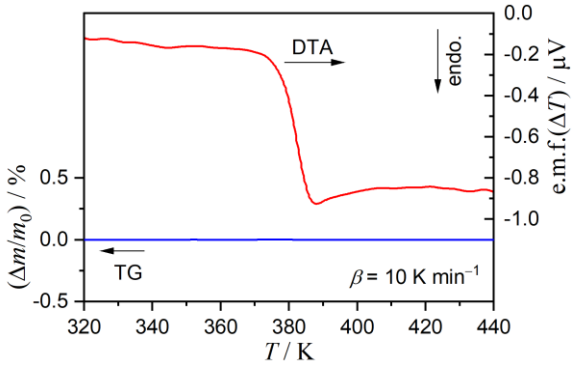

Figure S20. TG–DTA curves recorded by heating the sample obtained by naturally cooling the liquid SPyrG produced by the thermal dehydration reactions of MSG-MH.

References

S1. Sano, C.; Nagashima, N.; Kawakita, T.; Iitaka, Y., Crystal and Molecular Structures of Monosodium L-Glutamate Monohydrate. *Anal. Sci.* **1989**, *5*, 121-122.